Journal of
Marine Science and Engineering

MDPI

Article

Experimental Study on the Ice Resistance of a Naval Surface Ship with a Non-Icebreaking Bow

Jianqiao Sun [1,2] and Yan Huang [1,2,3,*]

[1] School of Civil Engineering, Tianjin University, Tianjin 300350, China; sun1008@tju.edu.cn
[2] Tianjin Key Laboratory of Port and Ocean Engineering, Tianjin University, Tianjin 300350, China
[3] State Key Laboratory of Hydraulic Engineering Simulation and Safety, Tianjin University, Tianjin 300350, China
* Correspondence: hjacyky@tju.edu.cn

Abstract: With the shrinking of Arctic sea ice due to global climate change, potential access to Arctic waters has increased for non-typical icebreaking or strengthened ships. Numerous studies have been conducted on hull form designs and ice resistance predictions for ships with typical icebreaking bows, but published research for ships with non-icebreaking bows in ice is still rare. The objective of this study was to investigate the ice resistance of a naval surface ship with a non-icebreaking bow through model tests in an ice tank. The naval surface combatant concept DTMB 5415 was used as the ship model. The tests were conducted under different levels of ice thicknesses and speeds. During the tests, the total resistance of the model ship was measured, accompanied by monitoring of the ice load at the stem area with a flexible tactile sensor sheet. Compared with the test results of icebreaker models in former studies, the total ice resistance, as well as the stem ice load, of the present ship was significantly higher. The ice crushing resistance component in the stem area accounted for more than 60% of the total resistance in the ice. Discussions on the applicability of a semi-empirical formula for predicting the ice resistance of the present ship are also presented. Keinonen's formula was found to be relatively more consistent with the predictions produced by model tests, and a preliminary modification was proposed to obtain more accurate predictions.

Keywords: ice resistance; non-icebreaking bow; model test; ice load

check for updates

Citation: Sun, J.; Huang, Y. Experimental Study on the Ice Resistance of a Naval Surface Ship with a Non-Icebreaking Bow. *J. Mar. Sci. Eng.* **2023**, *11*, 1518. https://doi.org/10.3390/jmse11081518

Academic Editor: Joško Parunov

Received: 1 July 2023
Revised: 16 July 2023
Accepted: 24 July 2023
Published: 30 July 2023

Copyright: © 2023 by the authors. Licensee MDPI, Basel, Switzerland. This article is an open access article distributed under the terms and conditions of the Creative Commons Attribution (CC BY) license (https://creativecommons.org/licenses/by/4.0/).

1. Introduction

Global warming and the long decline of Arctic sea ice have contributed to the seasonal accessibility of the Northern Sea Route (NSR), producing new opportunities for non-icebreaking ships to navigate through ice-covered waters. From 2016 to 2020, a total of 617 ships passed through the NSR, of which 107 vessels were not assigned to an ice class [1]. In 2021, China COSCO Shipping Group arranged 14 transit voyages from Asia to Europe through the Arctic, 10 of which were independent navigations without an additional icebreaker escort [2]. The increasing number of military exercises in the Arctic by NATO and Russia in recent years [3–5] has also demonstrated the feasibility of non-icebreaking naval surface ships in ice-covered waters.

Opportunities are always accompanied by challenges. For non-icebreaking ships, sea ice is still the main obstacle that limits Arctic navigation. In the design of a bow shape for non-icebreaking purposes, resistance in calm water and seakeeping performance in waves are the main considerations, and the representative features may include a slender waterline profile, raked or inverted bow stem, moderate flare above the waterline, and the integration of bulbs below the waterline [5]. These features often do not satisfy the requirements of icebreaking and clearing. The flexural strength of sea ice is much smaller than the compressive strength [6]; therefore, the primary goal of an icebreaking bow design is to make the ice fail in a bending mode instead of crushing it. Accordingly, a typical

icebreaking bow has quite narrow stem angles, ranging from 20° to 28° [7,8]. Regarding simple ice bending failure, a bow shape of a downward sloping plane, similar to that of landing craft, may be more effective, such as those adopted in the early Waas bow concept [9] and the Swedish icebreaker Oden. On the other hand, to minimize hull–ice friction and the amount of ice sliding into the propeller area, the clearing of broken ice pieces aside is also required. In this regard, wedge- or spoon-shaped bows with small flare angles (measured from the horizontal) have been widely adopted among icebreaking ships [10].

Obviously, non-icebreaking ships can still be exposed to the risk of besetting caused by insufficient icebreaking and clearing capabilities due to the conflict in bow design, despite the decreasing Arctic sea ice thickness. Therefore, prior to independent navigation in ice-covered waters, a reasonable prediction of resistance for non-icebreaking ships is necessary for risk analysis and evaluation in ice. However, current empirical or semi-empirical methods for ice resistance calculation are mostly derived from the measured data of icebreaking ships [11]. The applicability of these empirical methods for non-icebreaking ships still needs to be verified due to the significant changes in bow form. Published studies regarding this issue, however, are very limited. Hisette et al. [12] performed a literature study of the existing methods for estimating the resistance of ships in ice and assessed the applicability of the Lindqvist method to vessels with conventional bow shapes. They pointed out that the Lindqvist formula provided reasonable values up to a stem angle of approximately 60–70°. Furthermore, Hisette and Myland [13] developed a methodology to identify and evaluate level ice resistance and its distribution along the hull of ships with non-typical icebreaking bow shapes using a segmented and highly instrumented model ship hull. Their tests provided insights on the hull–ice interactions of non-typical icebreaking ships under different draughts, and valuable data were published to reveal the influences of ship velocity and ice thickness on level ice resistance and its components [14].

In this context, a series of model tests were carried out in an ice tank to assess the level ice resistance of a naval surface ship with a non-icebreaking bow. The objectives of the present tests are as follows:

i. To assess the resistance of the present ship under relatively harsh level ice conditions and extend the database of the experimental results produced by former studies [14];
ii. To determine the icebreaking resistance component for the present non-icebreaking bow using tactile sensors, which have been applied to an icebreaking ship model by the authors in the previous study [15];
iii. To propose a preliminarily modified semi-empirical formula for the prediction of the ice resistance of the present ship based on test data.

2. Overview of the Model Tests

2.1. Test Facilities and Model Ice

The present tests were conducted in the Ice Mechanics and Engineering Laboratory of Tianjin University. The laboratory is a member of the International Towing Tank Conference (ITTC) and has an insulated cold room of 320 m^2 to accommodate ice tanks. The ice tank was 40 m in length, 6 m in width, and 2 m in depth, with model ice produced at temperatures of −25 to −22 °C. The main carriage was used for towing the ship model, which could operate at moving speeds of 0.001 to 1.0 m/s with towing forces up to 5 tons.

Model ice sheets were produced in the tank from an aqueous solution containing 1.5% urea. The model ice was grown in a seeding process, which was achieved by spraying a mist of aqueous urea solution with compressed air above the water surface. After the nucleation of ice on the water surface, the room temperature was lowered to −22 °C to achieve the desired ice thickness. Model ice grown through the above process was characterized by a columnar crystal structure, as shown in Figure 1. The strength of the model ice was controlled by tempering. A detailed description of the seeding process is presented in [16], and the mechanical properties of the present model ice are presented in [17].

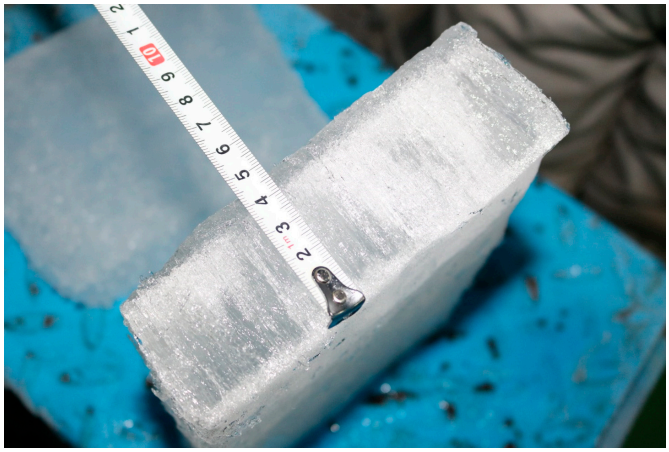

Figure 1. Section of the present model ice.

2.2. Scaling Laws

Froude and Cauchy scaling laws have been widely accepted in the physical modeling of ships breaking ice [16,18,19]. Ships navigate in level ice at a certain mass and speed, where gravity and inertia forces govern the process, and thus, the Froude similarity applies. Meanwhile, the ice sheet fails in local brittle crushing and bending, where elastic forces predominate, and the Cauchy similarity can be applied. The Froude number, Fr, and Cauchy number, Ca, can be calculated using:

$$Fr = \frac{V}{\sqrt{gL}} \tag{1}$$

$$Ca = \frac{\rho V^2}{E} \tag{2}$$

where V is the velocity, g is the acceleration of gravity, L is the geometric length, ρ is the density, and E is the elastic modulus of ice.

Based on the maintenance of Froude and Cauchy numbers in both full and model scales, ice thickness, strength and elastic modulus are scaled by λ (i.e., the geometric scale factor; set as 30 in the present tests), time and velocity are scaled by $\lambda^{1/2}$, and mass and force are scaled by λ^3.

Notably, the application of Cauchy scaling requires the material behavior of the ice to be linear elastic, and the crushing failure of ice is highly rate-sensitive with creep deformations at low strain rates and continuous brittle crushing at high strain rates [20,21]. Derradji-Aouat [22] proposed a sufficiently high strain rate for the linear elastic behavior of ice with a brittle mode of failure to be higher than 10^{-3} s^{-1}. For the present model ice, the transition strain rate from the ductile to brittle mode of failure was approximately $10^{-2.2}$ s^{-1}. For the present icebreaking scenario, the strain rate was estimated to be in the order of $10^{-1.3}$ s^{-1} to $10^{-0.6}$ s^{-1}, well above the transition rate; thus, Cauchy scaling could be suitable for the extrapolation of elastic forces generated in the ice crushing process.

2.3. Ship Model

In the present tests, the U.S. Navy surface combatant concept DTMB 5415 was used as the full-scale ship. The hull line of this ship are detailed in [23]; the main dimensions are listed in Table 1. The waterline and flare angles were measured at 1/4 B; B represents the ship breadth. This ship had a "clipper bow" form with a bulb below the waterline. Compared with typical icebreaking bows, the ship had larger stem and flare angles with respect to the horizontal, which may not have been sufficient to initiate downward bending failure of the ice sheet and the side clearing of broken ice pieces. The ship was propelled by two shaft propellers and had a service speed of 30 kn in open water. The geometric scale

factor of the model ship was 1:30. The outer surface of the model ship hull was painted, and the average kinetic friction coefficient between the model ice pieces and the painted model hull was measured to be approximately 0.10 at a sliding velocity of 100 mm/s under air temperature of −5 °C.

Table 1. Main dimensions of the DTMB 5415.

Item	Full-Scale	Model-Scale
Waterline length (m)	142.18	4.74
Waterline breadth (m)	19.06	0.64
Draught (m)	6.15	0.21
Stem angle (°)	68	68
Waterline angle (°)	14	14
Flare angle (°)	64	64

2.4. Test Procedure

The present tests were conducted under the ITTC recommended procedures and guidelines [24]. The ship model was towed through the ice sheet by the main carriage at required constant speeds, with free heave, pitch, and roll motions, and limited sway and yaw. For resistance tests, the propellers were treated as appendages with zero rotational rate. The towing force, therefore, was equal to the total resistance in the ice. Such force was measured by a load cell connecting the towing system and the model. To evaluate the icebreaking resistance component of the present ship, a flexible tactile sensor sheet was attached on the starboard side of the model ship covering the "ice belt" area from bow stem to shoulder. The surface of the sensor sheet was covered by waterproof tapes, which had nearly the same friction coefficient as the painted model hull. The sensor sheet was 1 m in length and 0.2 m in width, containing a grid of 32 × 20 sensing elements. The sample rate was 100 Hz, which might be low for ice crushing measurements. However, former laboratory experiments using the same sampling rate have demonstrated the effectiveness of recording cyclic loads and time-varying pressure distributions during ice crushing process [25,26]. Considering that the resistance was defined as the time average of the measured longitudinal forces, the present sampling rate was regarded as an acceptable compromise between the data sufficiency and hardware cost.

The test runs were conducted immediately after the desired flexural strength of the model ice was reached. Then, the model ship was towed through the ice sheet at the required velocity. To determine the sufficiency and relatively steady state of the test data, the towing distance in each test run was set as four times the model ship length. For each test run, above- and underwater video cameras were used to record the breaking and submerging of the ice.

2.5. Test Conditions

This study assessed the level ice resistance of the present naval surface ship under different level ice thickness and ship velocities. The target conditions are detailed in Table 2. The full-scale ice thicknesses were selected as "Medium First Year Ice" [27] to assess the resistance of the present non-icebreaking ship under relatively harsh level ice conditions, which might exceed the icebreaking capacity of the present ship designed for open water navigations. Conversion between the model scale and full scale, following the Froude–Cauchy similarity. The target ice flexural strength was set as 500 kPa at the full scale; the corresponding model-scale value was 16.7 kPa. Since the bending moments in ice by the sloping hull shape generally originated from the local crushing of ice, the compressive strength of the present model ice was also measured. The ratio of compressive strength to flexural strength was 2.8, with a standard deviation of 0.4.

Table 2. Test conditions.

Test No.	Ice Thickness		Ship Velocity	
	Model-Scale (cm)	Full-Scale (m)	Model-Scale (mm/s)	Full-Scale (kn)
1	3.3	1.0	94	1
2			188	2
3			282	3
4	4.0	1.2	188	2
5			282	3
6			470	5

3. Icebreaking and Submerging Process

For ships with icebreaking bows, successive circumferential cracks of relatively large radii propagating from bow stem to shoulder and wedge-shaped broken ice pieces generated by the ice bending failure are typical features of icebreaking phenomena at the bow area [15]. For the present non-icebreaking bow, whether these features change or not was the focus of the experimental observation in this study.

Figure 2 presents the test scenes of the ship model navigating through the model ice sheet and backing out of the ice sheet, respectively. There were no obvious circumferential cracks from the bow stem to the shoulder during the breaking of ice, and ice failure at the bow area was quite close to the hull surface. After the model test was performed, the local ice sheet was found to be crushed into small cusps, and wedge-shaped broken ice pieces were not observed, which indicated that the ice failure mode at the bow area of the present ship was dominated by crushing.

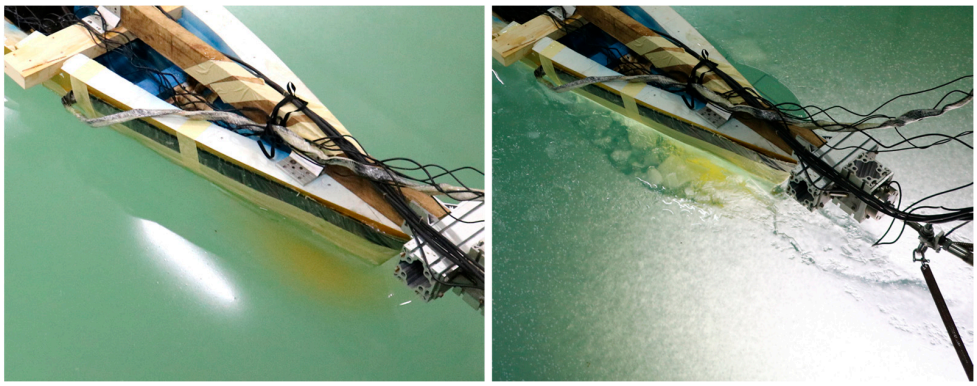

Figure 2. Ice failure at the bow area. No obvious circumferential cracks and the small broken ice pieces indicate a crushing type of ice failure.

As the ship advanced further, circumferential cracks in the ice sheet started to propagate from the bow shoulder to the midship, as shown in Figure 3. This indicated that the bow form of the present ship itself could not open an ice channel wider than the ship breadth; thus, the midship would be subjected to more lateral ice pressures, which, in turn, would produce additional friction to the ship.

Furthermore, submerging of the broken ice pieces along the bottom of the ship was observed by an underwater camera. Figure 4 shows a panoramic view of the distribution of the submerged ice pieces underneath the ship through three screenshots stitched together. The model ice was translucent, and the model ship had been smoothed and painted; therefore, the blurred areas of the bottom of the ship implied ice coverage. A rough estimate of the coverage of broken ice pieces underneath the ship was 85% or more, indicating relatively large submersion and frictional resistance in the ice. In addition, most of the broken ice pieces sliding along the ship bottom would finally make contact with the propellers, leading to frequent propeller–ice colliding and milling events, thus reducing the propulsion efficiency.

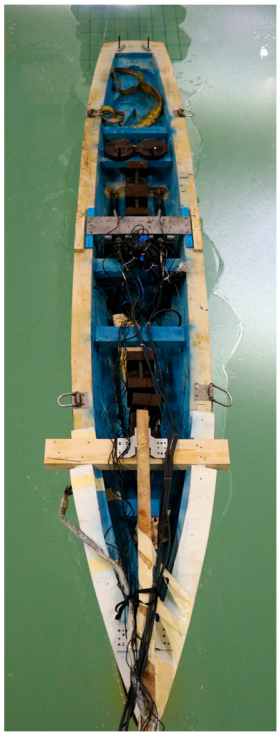

Figure 3. Ice failure generated by the circumferential cracks at the shoulder and midship area.

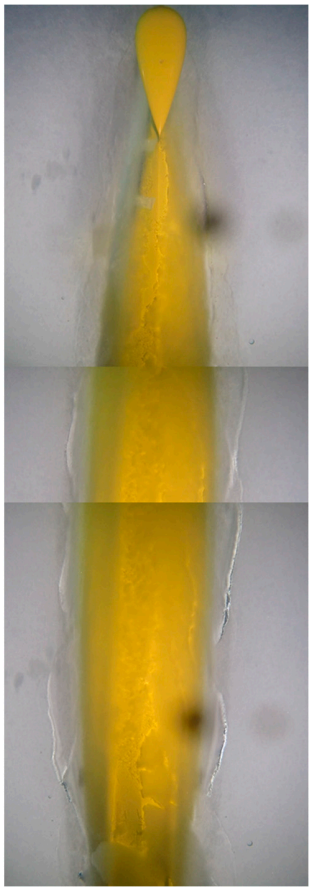

Figure 4. Underwater broken ice pieces along the bottom of the ship. The large broken ice pieces at the stern area indicate the insufficient ice clearing capacity of the present ship.

As a result of the observed phenomena, the present non-icebreaking bow form was found to be deficient in icebreaking and clearing capabilities, which indicated possibly higher resistance during the navigation in level ice compared with typical icebreaking ships.

4. Data Analyses and Discussion

4.1. Prediction of Total Resistance in Ice

Figure 5 presents the time history of towing force on the ship model through the model ice sheet for test no. 6, corresponding to the full-scale ice thickness of 1.2 m and ship velocity of 5 kn. According to the ITTC Recommended Procedures [24], the total ice resistance is defined as the time average of the longitudinal force resisting the motion of the ship, and the time interval has to be of sufficient length to achieve a steady state, with transient effects minimized and the fully developed flow of ice around the hull. This state is usually established after one model ship length. By calculating the average value of the towing force after one model length into the ice sheet, the total resistance of the model ship under this ice thickness and velocity could be obtained, and then the full-scale resistance could be predicted by the Froude–Cauchy similarity (i.e., multiplied by λ^3; $\lambda = 30$ for the present tests). Figure 6 gives the variation in the predicted total resistance with ice thickness and ship velocity for the full scale. Additionally, the predicted resistance of the Chinese polar research vessel RV Xuelong with a wedge-shaped icebreaking bow in some of the same ice conditions was used as a magnitude reference, which was obtained from previous model tests performed at Tianjin University [28].

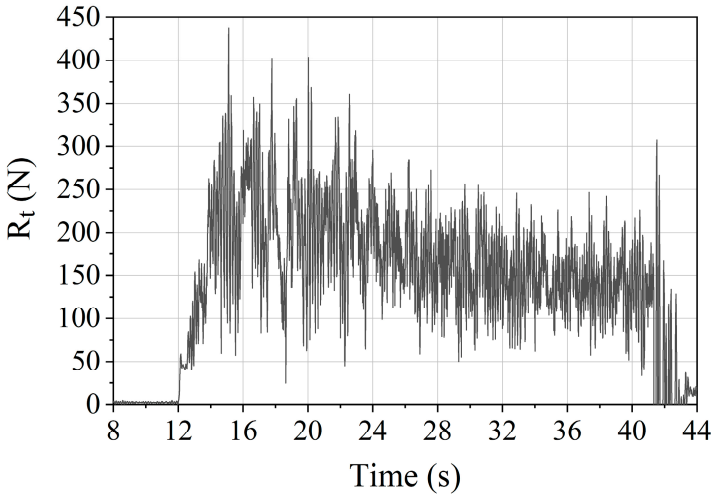

Figure 5. Time history of the measured total ice resistance of the present ship from test no. 6 in model scale. The full-scale ice conditions correspond to an ice thickness of 1.2 m and ship velocity of 5 kn.

Notably, the present ship, DTMB 5415, is smaller than the RV Xuelong in terms of length, breadth and draught, and the former's displacement is nearly o1ne-third of the latter. However, the ice resistance of the present ship under the same conditions is much higher than that of the Xuelong: the resistance at 1.0 m of ice thickness and 3 kn of ship velocity is close to 1.5 times that of the Xuelong, and the resistance of the present ship features a quite larger slope with the velocity. Such a comparison further verifies the greater resistance caused by the lack of icebreaking and clearing capabilities of the present non-icebreaking bow form.

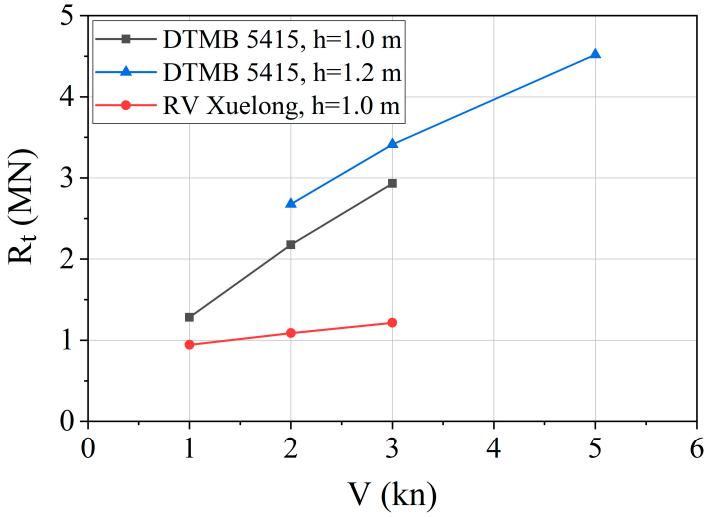

Figure 6. Prediction of the total ice resistance of the present ship and comparison with previous experimental results of the polar research vessel RV Xuelong in full scale.

4.2. Breaking Resistance Component by Tactile Sensor Data

As proposed by Lindqvist [29], the total ice resistance for icebreaking ships can be divided into breaking and submersion. For the present tests, the tactile sensor sheet provided direct measurements regarding the ice crushing pressure on the model hull surface, as displayed in Figure 2. Thus, the spatial variation in the ice pressure on the bow and its temporal variations could be recorded, quantified, and displayed. Figure 7 presents the spatial and temporal variations in the normal ice forces on the waterline of the covered bow area obtained from test no. 6. The *x*-axis, "Sub-area No.", represents the local positions corresponding to the sensing elements at the waterline area, where no. 3 is at the bow stem and no. 31 is near the shoulder, precisely 0.2 *L* from the forward perpendicular (*L*: the model ship length). Each "sub-area" contains the sum of ice pressures from eight sensing elements along the direction of ice thickness and the downward deformation of the ice sheet. Detailed data processing methods of the tactile sensor are presented elsewhere [15].

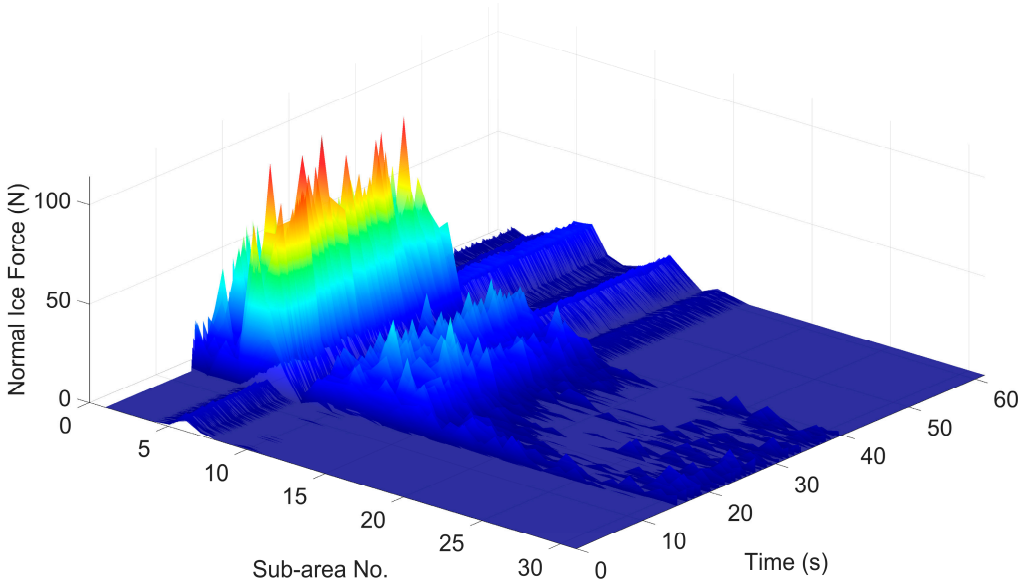

Figure 7. Spatial and temporal variations in the normal ice forces from test no. 6 in model scale. Sub-area no. 3 represents the bow stem, and no. 31 represents the near shoulder.

The ice load at the stem area featured a kind of continuous fluctuation similar to the pattern of continuous ice crushing. After the normal ice force had been converted to the average pressure, i.e., divided by the total area of the sensing elements in each "sub-area", the peak values were found to be approximately 2.4 times greater than the flexural strength of the model ice, which was close to the compressive strength. The above features indicate that the brittle crushing governed the failure process of the ice at the stem area. On the other hand, the normal ice loads near the shoulder area were quite small. The intermittent loading pattern of the temporal variation near the shoulder indicated a bending type of ice failure, which corresponds to the phenomenon presented in Figure 3. Unfortunately, ice loads at the rear part of the bow shoulder and the midship were not measured due to the limited length of the sensor sheet.

The ice forces induced by the crushing failure at the stem area were significantly larger than those on the rest of the bow (see Figure 7); therefore, the ice crushing resistance component was focused. To obtain the ice crushing resistance at the stem, the first step was to determine the extent of the stem area. According to the rules established by Det Norske Veritas (DNV) [30], the stem area is defined by the part of the bow area between the stem line and a line 0.06 L aft of the stem line or 0.125 B outboard from the center line, whichever is first reached. For the present test, the stem area corresponded to sub-area no. 3 to 13 on the tactile sensor sheet. Such areas also covered the ice crushing zone, according to Figure 7. Secondly, the normal ice forces were converted to the horizontal plane and the direction of advance. For the present tactile sensor data, conversions between the ice crushing resistance and the normal ice forces were calculated using:

$$R_c(t) = \sum_{i=3}^{13} F_i(t) \times \sin \alpha_i \times \cos \beta_i' \times 2 \tag{3}$$

where R_c represents the ice crushing resistance component, F_i represents the normal ice force at sub-area no. i, α represents the waterline angle, β' represents the normal frame angle (with respect to the vertical), and t represents the time. The coefficient "2" was based on the assumption that the ice sheet failed simultaneously on both sides of the bow. Such calculating methods have been applied to the evaluation of breaking resistance components in previous tests [15]. Figure 8 presents the time history of the ice crushing resistance of test no. 6 derived from the spatial and temporal variations in the normal ice forces in Figure 7. As with the total resistance, the average value after one model length into the ice sheet was calculated, scaled up, and used as the ice crushing resistance component.

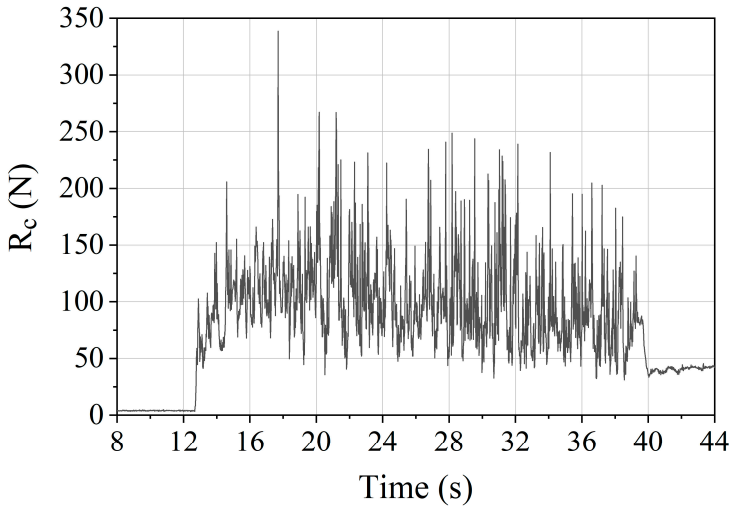

Figure 8. Time history of the ice crushing resistance at the stem area obtained from the tactile sensor data of test no. 6 in model scale.

Figure 9 presents the predicted total resistance and the ice crushing component of the present ship in full scale. The variations in the R_c-to-R_t ratio with ice thickness and ship velocity are plotted in Figure 10. Compared with the breaking proportion for typical icebreaking ships, which might be 40% to 50% for medium or large ships [12,15,31], the ice crushing resistance of the present non-icebreaking bow form accounted for 60% to 80% of the total resistance, with higher percentages for thinner ice conditions. Additionally, an overall decreasing trend was observed with the increasing ship velocity, which might have resulted from the increasing ice coverage underneath the ship due to delayed ice clearing at higher velocities. As mentioned above, the primary goal of an icebreaking bow design is to make the ice fail in a bending mode instead of crushing. The results from Figure 10 indicate that the non-icebreaking bow is still not suitable for breaking the level ice under the background of shrinking Arctic ice cover. Considering that naval surface ships generally have much more propulsion power than icebreaking ships similar in size, the hull structure should be further strengthened before navigating in ice-covered area alone.

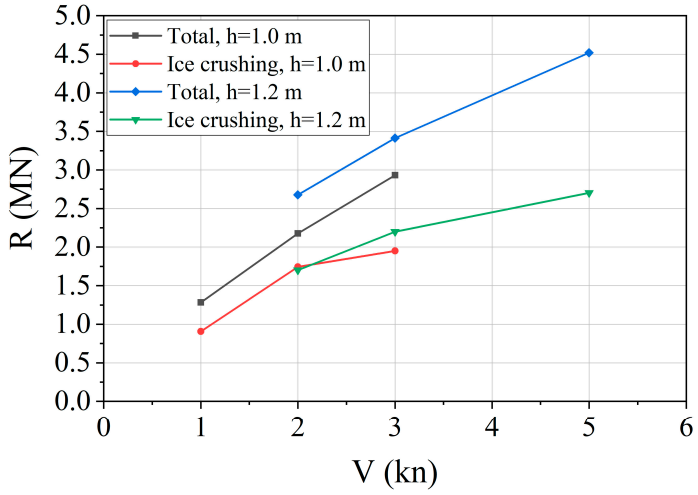

Figure 9. The predicted total and ice crushing resistance of the present ship at full scale.

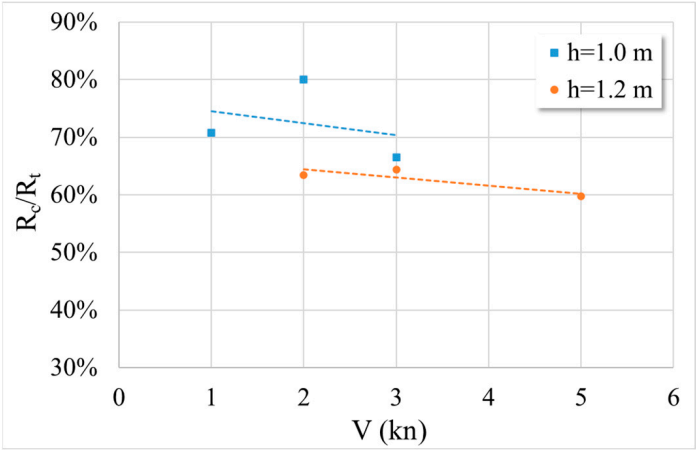

Figure 10. Variation in the ratio of the ice crushing resistance component, R_c, to the total resistance, R_t, with ice thickness and ship velocity.

4.3. Discussions on the Applicability of Empirical Formulas

As mentioned earlier, considerable research has been carried out for the full-scale measurements of ice resistance for icebreaking ship types; Enkvist [32], Lindqvist [29], Keinonen [33,34], Riska [35], Spencer [36], and others have established several empirical or semi-empirical formulas for the prediction of ice resistance based on varied ice trial data.

These empirical formulas have usually considered ice thickness, ice strength, ice density, ship dimensions, velocity, etc., as basic variables; some of them have also included hull form parameters, such as stem angle and flare angle.

Before using the existing empirical formulas for comparison, a preliminary selection was made according to the characteristics of the non-icebreaking ship type. As mentioned above, the clearest distinction between non-icebreaking and icebreaking ships is reflected in the bow form. If the empirical formula derived from icebreaking ships were to be directly applied to non-icebreaking ships, the formula should include the hull angles as variables. Otherwise, there would be no difference in the calculated results under the same ship dimensions and ice conditions. Therefore, Lindqvist, Riska, and Keinonen's formulas were selected to calculate the total resistance of the present ship, DTMB 5415, in the ice. Among them, Lindqvist's formula contained three hull form parameters: stem angle, waterline angle, and flare angle; Riska's formula included only one form parameter, i.e., stem angle, but two ship dimension parameters of bow length and midship length were added; Keinonen's formula considered stem and flare angles as input. Detailed expressions of these formulas are presented elsewhere [29,32–36].

Comparisons of the calculated results of ice resistance using these three empirical formulas with the results predicted by the present model tests are shown in Figure 11. Generally speaking, the three selected empirical formulas underestimate the ice resistance of the present non-icebreaking ship. Ice resistance calculated by Riska's formula features the flattest slope and lowest value. In comparison, the calculated results of Keinonen's formula are more consistent with the predicted results by the present tests. However, it should be mentioned that the Keinonen's formula still underestimates the total resistance at an ice thickness of 1.0 m and ship velocity of 3 kn by approximately 16%, and such underestimation might become larger as the velocity continues to increase. Thus, it is still necessary to research modifications of the traditional empirical formulas in order to achieve a more reasonable assessment of ice resistance for non-icebreaking ship types.

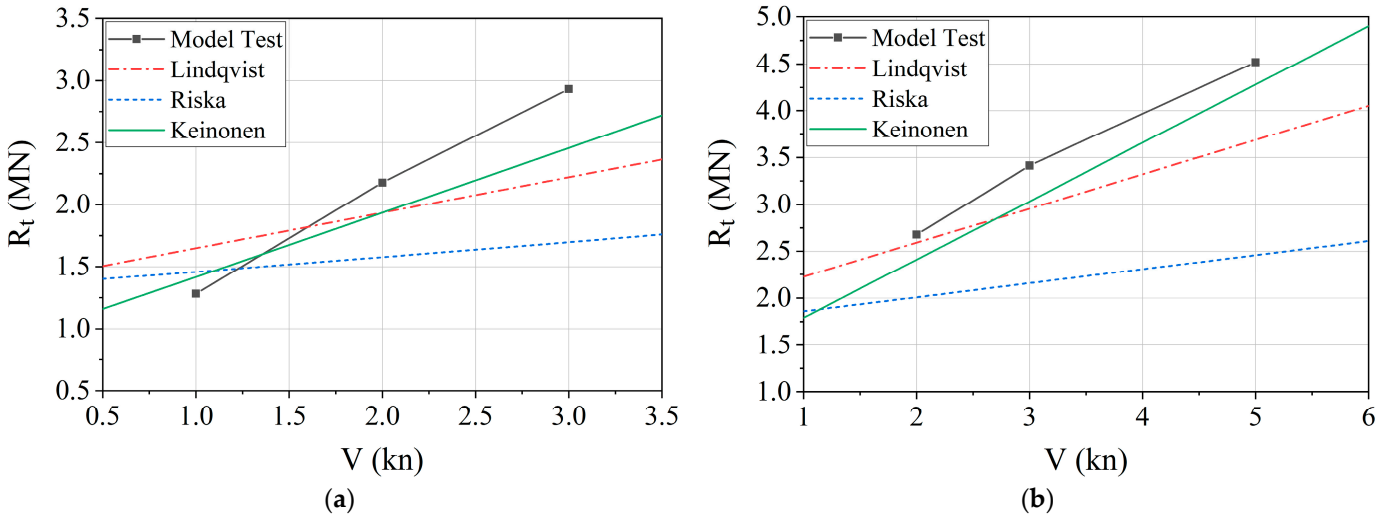

Figure 11. Comparison of the predicted ice resistance based on empirical formulas and model tests: (**a**) for an ice thickness of 1.0 m; (**b**) for an ice thickness of 1.2 m.

As a preliminary attempt, the present study made simple modifications to the original Keinonen's formula to obtain a more accurate prediction with respect to the test results. The original Keinonen's formula can be expressed by:

$$\begin{aligned} R_1 \quad &= 0.08 + 0.017 \cdot C_s \cdot C_h \cdot B^{0.7} \cdot L^{0.2} \cdot T^{0.1} \cdot h^{1.25} \cdot \\ &[1 - 0.0083(t + 30)] \cdot \left[0.63 + 0.00074 \cdot \sigma_f\right] \cdot \\ &\left[1 + 0.0018(90 - \psi)^{1.4}\right] \cdot \left[1 + 0.004(\varphi - 5)^{1.5}\right] \end{aligned} \tag{4}$$

$$\begin{aligned}\Delta R &= 0.009 \cdot \tfrac{\Delta V}{\sqrt{gL}} \cdot C_h \cdot B^{1.5} \cdot L^{0.5} \cdot h \cdot \\ &[1 - 0.0083(t + 30)] \cdot \\ &\left[1 + 0.0018(90 - \psi)^{1.4}\right] \cdot \left[1 + 0.003(\varphi - 5)^{1.5}\right]\end{aligned} \tag{5}$$

where R_1 is the level ice resistance at a speed of 1 m/s; ΔR represents an increase in ice resistance above that at 1 m/s; ΔV is the increase in ship velocity above 1 m/s; C_s is the salinity correction coefficient (1.0 for saline ice); C_h is the hull condition correction coefficient (1.0 for the Inerta coating); B, L, and T are the ship breadth, length and draught, respectively; h and σ_f are the ice thickness and flexural strength, respectively; t is the air temperature (-15 °C); and ψ and φ are the average flare and buttock angles over the bow, respectively. The expression for chined bow shoulders was used in the present study due to the reduced scatter in the original data fitting stated by Keinonen [33].

As mentioned above, the calculated results by Keinonen's formula were generally insufficient in value and slope. Thus, the coefficient of 0.017 was related to the absolute value of R_1 and the exponent for the nondimensionalized ΔV (i.e., $\frac{\Delta V}{\sqrt{gL}}$) related to the slope of the resistance with velocity were determined to be modified. As the slopes for ice thicknesses of 1.0 m and 1.2 m were slightly different, the exponent for the nondimensionalized ΔV was assumed to be a function of ice thickness and expressed by a linear relationship with the slope for ice thickness of 1.2 m unchanged:

$$\eta_V = 0.5 \cdot h + 0.4 \tag{6}$$

where η_V represents the exponent for the nondimensionalized ΔV. Subsequently, the coefficient of 0.017 was further modified to 0.019 by iterative approximation. The modified Keinonen's formula was expressed by:

$$\begin{aligned}R_1 &= 0.08 + \mathbf{0.019} \cdot C_s \cdot C_h \cdot B^{0.7} \cdot L^{0.2} \cdot T^{0.1} \cdot h^{1.25} \cdot \\ &[1 - 0.0083(t + 30)] \cdot \left[0.63 + 0.00074 \cdot \sigma_f\right] \cdot \\ &\left[1 + 0.0018(90 - \psi)^{1.4}\right] \cdot \left[1 + 0.004(\varphi - 5)^{1.5}\right]\end{aligned} \tag{7}$$

$$\begin{aligned}\Delta R &= 0.009 \cdot \left(\tfrac{\Delta V}{\sqrt{gL}}\right)^{\mathbf{0.5}h\mathbf{+0.4}} \cdot C_h \cdot B^{1.5} \cdot L^{0.5} \cdot h \cdot \\ &[1 - 0.0083(t + 30)] \cdot \\ &\left[1 + 0.0018(90 - \psi)^{1.4}\right] \cdot \left[1 + 0.003(\varphi - 5)^{1.5}\right]\end{aligned} \tag{8}$$

where the modifications are written in bold. Table 3 lists the resistance values calculated by the original and modified Keinonen's formula with the error. Clearly, the above simple modifications could reduce the prediction error from 11% on average to 2%.

Table 3. Resistance calculated using the original and modified Keinonen's formula.

h (m)	V (kn)	Resistance by Model Test (MN)	Resistance by Keinonen (MN)			
			Original	Error	Modified	Error
1.0	1	1.281	1.416	11%	1.364	6%
	2	2.178	1.936	11%	2.181	0%
	3	2.931	2.456	16%	2.960	1%
1.2	2	2.678	2.409	10%	2.679	0%
	3	3.414	3.033	11%	3.303	3%
	5	4.521	4.280	5%	4.550	1%

5. Conclusions

In this study, a series of scaled model tests was conducted in an ice tank to assess the level ice resistance of the naval surface ship DTMB 5415 with a non-icebreaking bow form. The following conclusions can be drawn from the present tests:

i. The ice failure mode at the bow of the present ship was dominated by brittle crushing, which was significantly different from the bending failure caused by typical icebreaking bow forms. The ice crushing resistance component at the stem area could account for over 70% of the total resistance according to the tactile sensor data, which was also undesirable when considering the strength of the local hull structure.
ii. The ice clearing capacity of the present ship was insufficient, leading to the ice coverage at the ship bottom being 85% or more, and a large number of broken ice pieces had drifted to the propeller area, which would finally reduce the propulsion efficiency.
iii. The ice resistance of the present ship varied more steeply with velocity, which could be reflected by the comparisons with the ice resistance of RV Xuelong and those from the empirical formulas. The calculated results of Keinonen's formula were relatively more consistent with the predictions from the model tests, but there was still a certain degree of underestimation. Simple modifications were proposed in the present study to the coefficient for R_1 and the exponent for the nondimensionalized ΔV, which could obtain a more accurate prediction.

Notably, the above conclusions are based on limited model tests for only one non-icebreaking ship type. The proposed modifications to the empirical formula may be rather tentative and only valid for similar ship types under close ice conditions. Experiments on other non-icebreaking bow forms are still needed in future studies.

Author Contributions: Conceptualization, Y.H.; methodology, Y.H. and J.S.; software, J.S.; validation, J.S.; formal analysis, J.S.; investigation, J.S.; resources, Y.H.; data curation, J.S.; writing—original draft preparation, J.S.; writing—review and editing, J.S. and Y.H.; visualization, J.S.; supervision, Y.H.; project administration, Y.H.; funding acquisition, Y.H. All authors have read and agreed to the published version of the manuscript.

Funding: This study has been financially supported by the National Natural Science Foundation of China (Grant Nos. 52192690, 52192691, 52192695, and 52101327) and the High-tech Ship Projects of the Ministry of Industry and Information Technology of China (Grant No. 2021-342).

Institutional Review Board Statement: Not applicable.

Informed Consent Statement: Not applicable.

Data Availability Statement: Not applicable.

Acknowledgments: The authors would like to thank the unknown reviewers who provided excellent guidance.

Conflicts of Interest: The authors declare no conflict of interest.

References

1. CHNL Information Office. Analyses of Shipping Traffic in the NSR Waters in 2020. Nord University, Bodø, Norway. Available online: https://arctic-lio.com/analysys-of-shipping-traffic-in-the-nsr-waters-in-2020/ (accessed on 28 August 2021).
2. Yang, F. Navigation Analysis and Suggestions of the Arctic Northeast Route. *China Marit. Saf.* **2022**, *8*, 69–72. (In Chinese)
3. Thompson-Jones, M. NATO's Arctic Exercise Is a Good Start to Standing Up to Russian Militarization of the High North. The National Interest Blog. Available online: https://nationalinterest.org/blog/buzz/natos-arctic-exercise-good-start-standing-russian-militarization-high-north-35367 (accessed on 6 November 2018).
4. Eckstein, M.U.S. U.K. Surface Warships Patrol Barents Sea for First Time Since the 1980s. USNI News. Available online: https://news.usni.org/2020/05/04/u-s-u-k-surface-warships-patrol-barents-sea-for-first-time-since-the-1980s (accessed on 4 May 2020).
5. Schneekluth, H.; Bertram, V. *Ship Design for Efficiency and Economy*, 2nd ed.; Butterworth-Heinemann: Oxford, UK, 1998.
6. Timco, G.W.; Weeks, W.F. A review of the engineering properties of sea ice. *Cold Reg. Sci. Technol.* **2010**, *60*, 107–129. [CrossRef]
7. Riska, K. Design of Ice Breaking Ships. In *Encyclopedia of Life Support Systems (EOLSS)*; EOLSS Publishers: Oxford, UK, 2010.
8. Myland, D.; Ehlers, S. Influence of bow design on ice breaking resistance. *Ocean. Eng.* **2016**, *119*, 217–232. [CrossRef]

9. Wilckens, H.; Freitas, A. Thyssen-Waas icebreaker concept model tests and full scale trials. *Cold Reg. Sci. Technol.* **1983**, *7*, 285–291. [CrossRef]
10. Jones, S.J. A history of icebreaking ships. *J. Ocean. Technol.* **2008**, *3*, 53–74.
11. Erceg, S.; Ehlers, S. Semi-empirical level ice resistance prediction methods. *Ship Technol. Res.* **2017**, *64*, 1–14. [CrossRef]
12. Hisette, Q.; Myland, D.; Müller, F.; Suominen, M. Investigations on the level ice resistance of ships with conventional bow shapes. In Proceedings of the 29th International Ocean and Polar Engineering Conference (ISOPE), Honolulu, HI, USA, 16–21 June 2019.
13. Hisette, Q.; Myland, D. Methodology to investigate the icebreaking process of ships with non-typical icebreaking bow shapes. In Proceedings of the ASME 2020 39th International Conference on Ocean, Offshore and Arctic Engineering (OMAE), Virtual, 3–7 August 2020.
14. Myland, D.; Hisette, Q. Experimental investigations on the level ice resistance of ships with non-typical icebreaking bow shapes. *Ships Offshore Struct.* **2021**, *16* (Suppl. S1), 225–236. [CrossRef]
15. Huang, Y.; Huang, S.; Sun, J. Experiments on navigating resistance of an icebreaker in snow covered level ice. *Cold Reg. Sci. Technol.* **2018**, *152*, 1–14. [CrossRef]
16. ITTC. General Guidance and Introduction to Ice Model Testing. In *ITTC Recommended Procedures and Guidelines*; International Towing Tank Conference: Zurich, Switzerland, 2021.
17. Sun, J.; Huang, Y. Investigations on the ship-ice impact: Part 1. *Exp. Methodologies. Mar. Struct.* **2020**, *72*, 102772. [CrossRef]
18. Timco, G.W. Ice forces on structures: Physical modeling techniques. In Proceedings of the IAHR Symposium on Ice, Hamburg, Germany, 27–31 August 1984; Volume 4, pp. 117–150.
19. *ISO 19906*; Petroleum and Natural Gas Industries—Arctic Offshore Structures. International Organization for Standardization: Geneva, Switzerland, 2019.
20. Schulson, E.M.; Buck, S.E. The ductile-to-brittle transition and ductile failure envelopes of orthotropic ice under biaxial compression. *Acta Metall. Mater.* **1995**, *43*, 3661–3668. [CrossRef]
21. Sodhi, D.S.; Takeuchi, T.; Nakazawa, N.; Akagawa, S.; Saeki, H. Medium-scale indentation tests on sea ice at various speeds. *Cold Reg. Sci. Technol.* **1998**, *28*, 161–182. [CrossRef]
22. Derradji-Aouat, A. Multi-surface failure criterion for saline ice in the brittle regime. *Cold Reg. Sci. Technol.* **2003**, *36*, 47–70. [CrossRef]
23. SIMMAN. US Navy Combatant, DTMB 5415 Geometry and Conditions. 2008. Available online: http://www.simman2008.dk/5415/combatant.html (accessed on 26 September 2022).
24. ITTC. Resistance Tests in Ice. In *ITTC Recommended Procedures and Guidelines*; International Towing Tank Conference: Zurich, Switzerland, 2021.
25. Wells, J.; Jordaan, I.; Derradji-Aouat, A.; Taylor, R. Small-scale laboratory experiments on the indentation failure of polycrystalline ice in compression: Main results and pressure distribution. *Cold Reg. Sci. Technol.* **2011**, *65*, 314–325. [CrossRef]
26. Määttänen, M.; Marjavaara, P.; Saarinen, S.; Laakso, M. Ice crushing tests with variable structural flexibility. *Cold Reg. Sci. Technol.* **2011**, *67*, 120–128. [CrossRef]
27. WMO. *Sea Ice Nomenclature*; Publication No. 259; World Meteorological Organization: Geneva, Switzerland, 2014.
28. Huang, Y. *Ship Model Tests under Continuous Icebreaking Mode*; Report for High-tech Ship Projects; Tianjin University: Tianjin, China, 2019. (In Chinese)
29. Lindqvist, G. A straightforward method for calculation of ice resistance of ships. In Proceedings of the 10th International Conference on Port and Ocean Engineering under Arctic Conditions (POAC), Luleå, Sweden, 12–16 June 1989; pp. 722–735.
30. DNV. Ships for Navigation in Ice. In *Rules for Classification of Ships*; Part 5, Chapter 1; Det Norske Veritas AS: Oslo, Norway, 2013.
31. Enkvist, E. A survey of experimental indications of the relation between the submersion and breaking components of level ice resistance to ships. In Proceedings of the 7th International Conference on Port and Ocean Engineering Under Arctic Conditions, Helsinki, Finland, 5–9 April 1983; Volume 1, pp. 484–493.
32. Enkvist, E. *On the Ice Resistance Encountered by Ships Operating in the Continuous Mode of Icebreaking*; Report No. 24; The Swedish Academy of Engineering Sciences in Finland: Helsinki, Finland, 1972.
33. Keinonen, A.; Browne, R.P.; Revill, C.R.; Bayly, I.M. Icebreaker performance prediction. *SNAME Trans.* **1991**, *99*, 221–248.
34. Keinonen, A.J.; Browne, R.P.; Revill, C.R.; Reynolds, A. *Icebreaker Characteristics Synthesis*; Report for Transportation Development Centre, Transport Canada, TP 12812E; AKAC Inc.: Victoria, BC, Canada, 1996.
35. Riska, K.; Wilhelmson, M.; Englund, K.; Leiviskä, T. *Performance of Merchant Vessels in Ice in the Baltic*; Research Report No. 52; Winter Navigation Research Board: Helsinki, Finland, 1998.
36. Spencer, D.; Jones, S.J. Model-Scale/Full-Scale Correlation in Open Water and Ice for Canadian Coast Guard "R-Class" Icebreakers. *J. Ship Res.* **2001**, *45*, 249–261. [CrossRef]

Disclaimer/Publisher's Note: The statements, opinions and data contained in all publications are solely those of the individual author(s) and contributor(s) and not of MDPI and/or the editor(s). MDPI and/or the editor(s) disclaim responsibility for any injury to people or property resulting from any ideas, methods, instructions or products referred to in the content.